Control-oriented modeling and analysis of tubular dielectric elastomer actuators dedicated to cardiac assist devices*

Ning Liu[1], Thomas Martinez[1], Armando Walter[1], Yoan Civet[1], and Yves Perriard[1]

***Abstract*— This paper deals with the control-oriented modeling of a multilayered dielectric elastomer actuator based tube. The actuator is clamped at both sides and performs a radial displacement. The hyperelastic deformation and the viscoelastic performance, together with the electro-mechanical coupling are considered in the model. With the chosen Yeoh's model for the Helmholtz free energy function, we aim to model the snap-through effect of this tubular actuator at high applied voltage. Simulation results of the nonlinear dynamic model are later compared with experimental ones in order to identify unknown parameters of the dielectric elastomer, especially to fit the snap-through effect and the high frequency performance. With proper identification process, our model has a good accuracy to fit the physical system (more than 90.27% for a ramp input and more than 82.7% for a step input) and is ready for the future controller design.**

***Index Terms*— Soft robotics, bio-medical robotics, dielectric elastomer actuators, modeling and identification.**

I. INTRODUCTION

Dielectric elastomer actuators (DEAs) were firstly introduced in [1] as a type of electro-active polymer (EAP) actuators. It is composed of a dielectric elastomer surrounded by two compliant electrodes. With an applied electric field, the generated Maxwell stress makes the elastomer squeeze along the thickness direction and expand in area, leading to a large deformation. The DEAs have advantages of fast response time, large deformation (the actuation strain usually goes up to 100%) with low density and low modulus compared to other kinds of EAP actuators (i.e. shape memory polymer actuators, ionic polymer metal composite actuators, etc.), making it a promising compliant actuator for soft robots, especially for the application of artificial muscles in the field of bio-medical robotics. Readers are referred to [2] for detailed reviews of the application of DEAs.

Among the applications, [3] has proposed to implement a tubular DEA with multilayers replacing part of the ascending aorta to treat the heart failure. The DEA is firstly pre-stretched under the internal pressure of the blood. With the voltage applied at the end of the diastole, the tubular DEA expands radially. On the other hand, the DEA is discharged at the end of the systole and contracts. As a result, this tubular DEA works as a soft robot. With the synchronization between this robot and the cardiovascular system, the implemented tubular DEA can better ease the deformation of the heart and support it to work properly. However, in order to activate the DEA with sufficient displacement, high voltages are required that may lead to electric field in the structure close to the breakdown limit of the DEA. One major factor of the breakdown in the DEA is the electro-mechanical instability (also known as snap-through effect). This instability comes from the relation between the electric field and the deformation of the DEA. With the electric field applied, the thickness of the DEA decreases and hence increases again the electric field, leading to potential breakdown of the DEA. This well-known phenomenon has been observed in the literature [4]–[6]. It has also been harnessed in [7] to design a giant high-speed soft actuator with a volume change of 1398% within 20 ms. When it comes to the present research of cardiac assist devices using the tubular DEAs, this giant high-speed deformation of DEAs is no longer a virtue. To avoid this instability, [8] put a rigid tube outside of the DEA in order to limit the radial displacement without triggering the snap-through effect. But this rigid protection prevents the maximum displacement and reduces attainable energy. In order to remove the rigid protection and to use the actuator in an optimal way without deterioration, we would like to stabilize the tubular DEA with a dynamic controller. As mentioned previously, the snap-through instability is due to the positive feedback between the electric field and the thickness of the DEA. From the control point of view, this positive feedback results in multiple equilibrium points of the DEA model [4], some of which are unstable. The use of a controller helps both to modify the stability of unstable equilibrium and to shape the close loop performance. As a first attempt, in this paper, we will focus on a tubular DEA with multilayers for the cardiac application and work on its dynamic modeling and the snap-through problem.

Up to now, various models of the DEAs have been proposed in the literature, most of which are static and are dedicated to material science, see [9]–[12] for example. In order to study the stability and the design of a controller, a dynamic DEA model is necessary. Compared to static models, the dynamic ones are more challenging with time dimension added. Moreover, the viscoelastic property should be considered to describe both the dissipation and the oscillation. In terms of the mathematical formulation, the dynamic models of DEAs can be divided into distributed parameter models and lumped parameter ones. The former is formulated by partial differential equations (PDEs), and simulates the dynamic properties precisely [13], [14]. However, these models are difficult regarding the numerical simulation and the controller implementation, because the PDEs need to be

*This work was supported by the Werner Siemens Foundation.

[1]Ning Liu, Thomas Martinez, Armando Walter, Yoan Civet, and Yves Perriard are with Integrated Actuators Laboratory, Ecole polytechnique fédérale de Lausanne, Switzerland. ning.liu@femto-st.fr, thomas.martinez@epfl.ch, yoan.civet@epfl.ch, armando.walter@epfl.ch, yves.perriard@epfl.ch.

properly approximated. To the best of our knowledge, there is no work on the controller design based on the distributed parameter models of the DEA in the literature. Different from the aforementioned one, the lumped parameter models first approximate the DEA into several segments under reasonable assumptions, and then propose dynamic models accordingly with ordinary differential equations. As a result, they are simpler for the simulation and controller design. The accuracy of the lumped parameter models can be improved by adding more segments. Many researches about the lumped parameter models of the DEA have been investigated, most of which deal with DEA strip [15], and conical DEAs [16]–[18]. The dynamic model of the rolled DEA tube has been investigated in [19] and [20], in which they work on the elongation of the DEA. Different from this existing model, we will focus on a more complicated configuration dedicated to the cardiac assist device where the DEA tube is clamped at two sides and generates radial deformation with the applied pressure and electric field. The circumferential force will also be considered in the model. Both the small deformation and the large snap-through deformation will be studied. Moreover, the contributions stem from the identification of the snap-through effect in the model. This modeling is necessary for the future controller design in order to achieve large deformation and to avoid the electro-mechanical instability.

The paper is organized as follows. Section II proposes the nonlinear dynamic model of the tubular DEA. For a first attempt, the tube will be simplified as a 1D model with one degree of freedom (DOF). The electro-mechanical coupling will be studied in the model. Identification of unknown parameters of the established model is performed in Section III. Comparisons between simulated and experimental results are also given. Finally, Section VI presents conclusions and perspectives.

II. Dynamic Modeling of the Tubular DEA

The models of the DEAs are multiphysical and consider both the mechanical deformation and the electrical part as well as their couplings. When it comes to our problem, the tubular DEA with multilayers is clamped at both sides, and will be pre-stretched with the inner pressure $p(t)$, and actuated with applied voltage $V(t)$, which are depicted in Fig. 1, with the zoom of the DEA on the right of the figure. The fabrication of the DEA with multilayers is detailed in [3]. A sectional view of the multilayers is illustrated in Fig. 2. It is firstly composed of four active layers of elastomer with positive and negative electrodes superimposed, which is presented in Fig. 2a. The initial thickness of each active layer is denoted by h_{ao}. This active layer is used to calculate the electric field. On the other hand, two passive layers are added and helps to protect the electrodes and to isolate the high input voltage in order to guarantee the safety when the tubular DEA will be implemented in the body in the future. The DEA is then rolled twice (cf. Fig. 2b) in order to improve the bonding of the actuator [8]. The initial thickness of the DEA tube is represented by h_o and will be used to calculate the mechanical deformation. We assume that the layers are ideally coated, such as no slipping happens during the deformation. The temperature is considered constant, so the thermal influence is neglected.

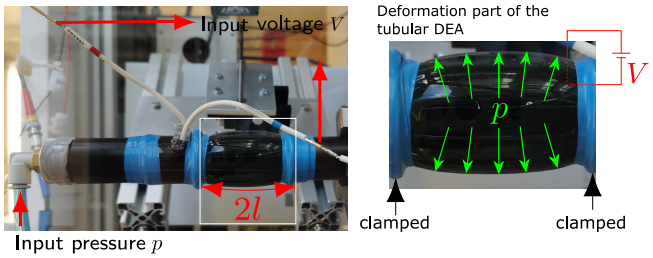

Fig. 1: Clamped-clamped multilayered tubular DEA.

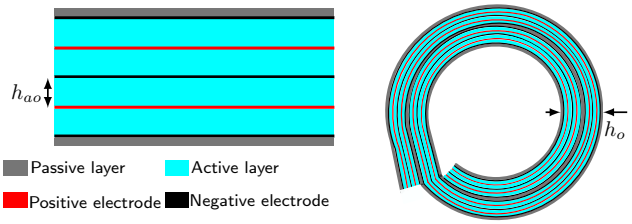

(a) Multilayered DEA before rolling.

(b) Multilayered DEA after two rolls.

Fig. 2: Section view of DEA multilayers before deformation.

Before modeling, we give the following assumptions:

Assumption 1: The material of the DEA is isotropic and incompressible.

Assumption 2: The elastomer is considered ideal, which means that the electric permittivity (i.e. the product of the vacuum permittivity ϵ_o and the relative dielectric permittivity ϵ_r) is a constant.

Assumption 3: The deformation is homogeneous and is supposed to be radial axisymmetric.

Assumption 4: There is no torsion in the tube. Only the flexion is taken into account.

From Assumption 3, the configuration of the tubular DEA in 3D as illustrated in Fig. 1 can be simplified as a 1D clamped-clamped membrane as presented in Fig. 3, where $2l_o$ denotes the initial longitudinal length, and $2l$ represents the length in the deformed configuration. h denotes the thickness of the DEA tube after deformation. r_o and R stand for the initial average radius and the deformed average radius of the tube, respectively. The tubular DEA undergoes its largest radial deformation at the center point, where the thickness is the thinnest due to the aforementioned incompressibility and the volume conservation law in Assumption 1. As a result, the snap-through instability would

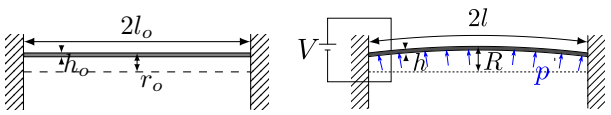

(a) Initial 1D configuration. (b) Deformed 1D configuration.

Fig. 3: Simplified 1D configurations of the DEA membrane.

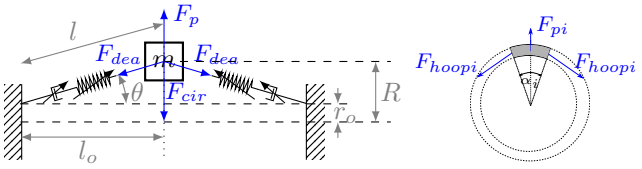

(a) Front view. (b) Side view.

Fig. 4: Simplified 1D model of the deformed DEA.

preferably occur around this point. For a first attempt, we only focus on the center point deformation of the tubular DEA. Therefore, the 1D membrane presented in Fig. 3b can again be simplified such as in Fig. 4, where m denotes the mass of the DEA, θ represents the deflection of the elastomer, F_p is the applied pressure force inside the tube, F_{dea} is the generated electro-mechanical force of the DEA tube in the longitudinal direction, F_{hoopi} represents the hoop force of the ith segments in the circumferential direction [21], and F_{cir} refers to the resultant circumferential force projected in the radial direction. Both F_{dea} and F_{hoopi} will be detailed in Subsection II-B and Subsection II-C, respectively.

A. Geometric configuration

We define the axial stretch λ_1, circumferential stretch λ_2 and thickness stretch λ_3 as: $\lambda_1(t) = l(t)/l_o$, $\lambda_2(t) = R(t)/r_o$, and $\lambda_3(t) = h(t)/h_o$. According to Assumption 1, the product among $\lambda_1(t)$, $\lambda_2(t)$ and $\lambda_3(t)$ follows:

$$\lambda_1(t)\lambda_2(t)\lambda_3(t) = 1. \tag{1}$$

We suppose that the active layer deforms the same way as the total thickness $h(t)$. Hence, we get the current thickness of the active layer h_a as:

$$h_a(t) = h_{ao}\lambda_3(t) = \frac{h_{ao}}{\lambda_1(t)\lambda_2(t)}. \tag{2}$$

With the relation giving $l^2(t) = l_o^2 + (R(t) - r_o)^2$, one can express $\lambda_1(t)$ as a function of $\lambda_2(t)$:

$$\lambda_1(t) = f(\lambda_2(t)) = \sqrt{1 + \frac{r_o^2}{l_o^2}(\lambda_2(t) - 1)^2}. \tag{3}$$

The angle $\theta(t)$ is calculated as follows:

$$\sin\theta(t) = \frac{R(t) - r_o}{l(t)} = \frac{r_o(\lambda_2(t) - 1)}{\sqrt{l_o^2 + (\lambda_2(t) - 1)r_o^2}}. \tag{4}$$

B. DEA force along the longitudinal direction

In this subsection we study the electro-mechanical force F_{dea} generated along the longitudinal direction of the DEA, which represents the coupling among the hyperelastic stress of the elastomer, the Maxwell stress generated by the electric field, the viscoelastic stress and the visco damper stress. This coupling was firstly modeled in [22] using the Prony series. Later [23] first proposed that this coupling can be represented analogously based on rheological elements with several springs and dampers. According to the literature, two main basic types of rheological models are used for the DEAs, e.g. the Kelvin-Voigt model [24] that consists of a spring and a damper in parallel, and the Zener model [16], [25]–[29] that is composed of a parallel combination of a spring with a spring-damper element in series. Other generalized rheological models have been proposed to get more precise information about the model, like the generalized Kelvin-Maxwell model [15], [18], [19], [30]–[32], which is a combination of the aforementioned Kelvin-Voigt model with spring-damper elements in parallel. We therefore apply the Generalized Kelvin-Maxwell model (cf. Fig. 5) to replace the nonlinear spring and damper as depicted in Fig. 4a. The upper spring-damper elements in parallel in Fig. 5 represent the viscoelastic stress σ_{vis}, the damper in parallel represents the visco damper stress σ_η and the nonlinear spring stands for the coupled hyperelastic stress and Maxwell stress in DEA along the longitudinal direction σ_m. The adding of σ_η comes from the experimental results. We have found that the simulation results with only σ_m and σ_{vis} do not fit the experimental measurements, especially regarding the response time and the initial oscillations. Furthermore, the addition of more viscoelastic elements does not improve the fitting. Therefore, we introduce the third visco damper stress and consider it as a linear term as a first attempt. Similar phenomenon has also been reported in [18]. The following part of this subsection will formulate these stresses in details.

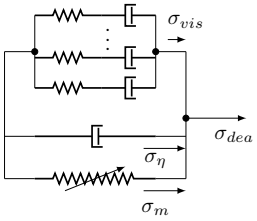

Fig. 5: Rheological representation of the stress σ_{dea} along the longitudinal direction.

a) Hyperelastic stress and Maxwell stress: The deformation of the elastomer is hyperelastic, which indicates that the relation between the mechanical stress and strain is no longer linear, and should be derived from the energy density function $W(\lambda_1, \lambda_2, \lambda_3, D)$, where D stands for the electric displacement. Because of the incompressibility in (1), $W(\lambda_1, \lambda_2, \lambda_3, D)$ can be reduced as a function that only depends on λ_1, λ_2 and D. For an ideal dielectric elastomer as supposed in Assumption 2, $W(\lambda_1, \lambda_2, D)$ is actually the sum of the Helmholtz free energy $W_s(\lambda_1, \lambda_2)$ and the electric charge energy, which is formulated as below:

$$W(\lambda_1, \lambda_2, D) = W_s(\lambda_1, \lambda_2) + \frac{D^2}{2\epsilon_o\epsilon_r}. \tag{5}$$

The relation between D and the electric field E is formulated as $D = \epsilon_o\epsilon_r E$, where E is calculated from the applied voltage as:

$$E = \frac{V}{h_a}. \tag{6}$$

Different formulations about the Helmholtz energy W_s exist in the literature. Here we apply the Yeoh's model [33] because of both its accuracy for large strain deformation and its simplicity with the reduced polynomial form, which can be expressed as follows:

$$W_s(\lambda_1,\lambda_2) = C_1\left(I_1-3\right) + C_2\left(I_1-3\right)^2 + C_3\left(I_1-3\right)^3, \tag{7}$$

where C_1, C_2 and C_3 are constitutive material parameters to be identified. From [33], the coefficient C_2 is negative and C_1 and C_3 are positive. I_1 denotes the first invariant of the left Cauchy-Green deformation that is written by $I_1 = \lambda_1^2+\lambda_2^2+1/\left(\lambda_1^2\lambda_2^2\right)$.

The stress σ_m is therefore calculated from $W(\lambda_1,\lambda_2,D)$ as in [9]:

$$\begin{aligned}\sigma_m &= \lambda_1\frac{\partial W_s}{\partial\lambda_1} - \epsilon_o\epsilon_r E^2\\ &= \lambda_1\left(C_1 + 2C_2\left(I_1-3\right) + 3C_3\left(I_1-3\right)^2\right)\frac{\partial I_1}{\partial\lambda_1} - \epsilon_o\epsilon_r E^2,\end{aligned} \tag{8}$$

with $\frac{\partial I_1}{\partial\lambda_1} = 2\lambda_1 - \frac{2}{\lambda_1^3\lambda_2^2} = 2f\left(\lambda_2\right) - \frac{2}{f(\lambda_2)^3\lambda_2^2}$.

b) Viscoelastic stress: The spring-damper elements in parallel at the top of Fig. 5 stand for the viscoelastic behavior of the DEA with its stress σ_{vis} formulated as:

$$\sigma_{vis} = \sum_{j=1}\sigma_{visj}, \tag{9}$$

with

$$\begin{aligned}\sigma_{visj} &= k_j\varepsilon_{kj} = \eta_j\dot{\varepsilon}_{\eta j},\\ \varepsilon_m &= \varepsilon_{kj} + \varepsilon_{\eta j},\end{aligned}$$

and

$$\begin{aligned}\dot{\sigma}_{visj} &= k_j\dot{\varepsilon}_{kj} = k_j\left(\dot{\varepsilon}_m - \dot{\varepsilon}_{\eta j}\right)\\ &= k_j\dot{\lambda}_1 - \frac{k_j}{\eta_j}\sigma_{visj} = k_j\frac{\partial\lambda_1}{\partial\lambda_2}\dot{\lambda}_2 - \frac{k_j}{\eta_j}\sigma_{visj},\end{aligned} \tag{10}$$

where k_j and η_j denote the stiffness and the damper coefficient of the jth parallel spring-damper element, respectively. ε_m, ε_{kj} and $\varepsilon_{\eta j}$ represent the strain deformation of the hyperelastic part, and of the jth viscoelastic part.

c) Visco damper stress: For the sake of simplicity, we first consider a linear relation for the visco damper stress σ_η in Fig. 5, which is formulated as:

$$\sigma_\eta = \eta_o\dot{\lambda}_1 = \eta_o\frac{\partial\lambda_1}{\partial\lambda_2}\dot{\lambda}_2, \tag{11}$$

where η_o represents the damping coefficient.

Therefore, the coupled electro-mechanical force F_{dea} generated in the DEA along the longitudinal direction is calculated by:

$$F_{dea} = \left(\sigma_m + \sigma_{vis} + \sigma_\eta\right)A_1, \tag{12}$$

with A_1 referring to the cross section area in the longitudinal direction of the tube, that is formulated as:

$$A_1 = \frac{2\pi r_o h_o}{f(\lambda_2)}. \tag{13}$$

C. DEA force along the circumferential direction

Besides the electro-mechanical force in the longitudinal direction, the tubular DEA generates also a force in the circumferential direction as illustrated in Fig. 4. F_{hoopi} is calculated from the hoop stress σ_{hoop}, which is formulated as:

$$\begin{aligned}\sigma_{hoop} &= \lambda_2\frac{\partial W_s}{\partial\lambda_2} - \epsilon_o\epsilon_r E^2\\ &= \lambda_2\left(C_1 + 2C_2\left(I_1-3\right) + 3C_3\left(I_1-3\right)^2\right)\frac{\partial I_1}{\partial\lambda_2} - \epsilon_o\epsilon_r E^2,\end{aligned} \tag{14}$$

with

$$\frac{\partial I_1}{\partial\lambda_2} = 2\lambda_2 - \frac{2}{\lambda_2^3\lambda_1^2} = 2\lambda_2 - \frac{2}{\lambda_2^3 f\left(\lambda_2\right)^2}.$$

The resultant circumferential force F_{cir} projected in the radial direction as illustrated in Fig. 4a gives:

$$F_{cir} = \sum_{i=1}^{n} 2\left(\sigma_{hoop}A_2\right)\sin\left(\frac{\alpha_i}{2}\right) \approx 2\pi\left(\sigma_{hoop}A_2\right), \tag{15}$$

with the cross section area A_2 calculated as $A_2 = hl$.

D. Equation of motion

According to Fig. 4, the equation of motion for the center point of the tube writes:

$$mr_o\frac{\mathrm{d}^2\lambda_2}{\mathrm{d}t^2}(t) = p(t)A_3(t) - 2F_{dea}(t)\sin\theta(t) - F_{cir}(t), \tag{16}$$

with $A_3(t) = 2\pi\left(r_o + R(t)\right)l(t)$ representing the inner surface area.

By choosing the state variables as follows:

$$\begin{aligned}x &= \begin{pmatrix}x_1 & x_2 & x_3 & \cdots & x_{j+2}\end{pmatrix}^T\\ &= \begin{pmatrix}\lambda_2 & \dot{\lambda}_2 & \sigma_{vis1} & \cdots & \sigma_{visj}\end{pmatrix}^T,\end{aligned} \tag{17}$$

and substituting (3), (6), (8), (10)-(15) into (16), the state space representation of the DEA dynamics is formulated as:

$$\dot{x}_1 = x_2, \tag{18a}$$

$$\begin{aligned}\dot{x}_2 = &-\frac{2}{mr_o}\left(\sigma_m(x_1,V) + \sum_j x_{j+2} + \sigma_\eta(x_1,x_2)\right)\\ &\cdot A_1(x_1)\sin\theta(x_1) - \frac{2\pi}{mr_o}\sigma_{hoop}(x_1,V)A_2(x_1)\\ &+ \frac{A_3(x_1)}{mr_o}p(t),\end{aligned} \tag{18b}$$

$$\dot{x}_3 = k_1\frac{\partial\lambda_1}{\partial x_1}x_2 - \frac{k_1}{\eta_1}x_3, \tag{18c}$$

$$\vdots$$

$$\dot{x}_{j+2} = k_j\frac{\partial\lambda_1}{\partial x_1}x_2 - \frac{k_j}{\eta_j}x_{j+2}. \tag{18d}$$

III. Parameters Identification of the Model

After the modeling of the tubular DEA, the parameters C_1, C_2, C_3, η_o, k_j and η_j in (18) are unknown and necessitate further identification to fit the experiment results. There is a trade-off between the model accuracy and the numerical simplicity, we thus choose $j = 2$ in (9), which indicates two pairs of spring-damper elements in Fig. 5. The dimensions of the DEA tube are listed in Table. I. The mass m of the tube is calculated from ρ and the volume.

TABLE I: Dimensions and known parameters of the DEA.

Names	Parameters	Values	Units
Length	l_o	24.5	mm
Radius	r_o	15	mm
Initial thickness	h_o	1	mm
Active layer	h_{ao}	100	µm
Volume density	ρ	10^3	$\mathrm{kg/m^3}$
Vacuum permittivity	ϵ_o	8.854×10^{-12}	F/m

The experimental setup is illustrated in Fig. 6. Both the active layers and passive layers of the DEA are silicone films (Elastosil 2030 from Wacker) with a thickness of 100 µm and 20 µm, respectively. The compliant electrodes are composed of LSR 4305 with carbon powder [3]. A pneumatic system imposes a pressure into the tubular DEA with the position of the piston, and a pressure sensor (Baumer) is used to measure it. The high voltage is generated by the voltage amplifier (Trek) and applied to the DEA tube. Both the profiles of the pressure and voltage are controlled in Labview. The radial deformation of the tubular DEA is measured by the 2D laser (Gocator).

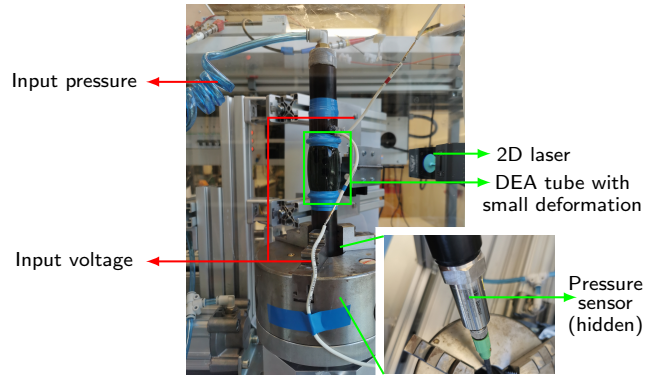

Fig. 6: Experimental setup of the tubular DEA under measurement.

We first identify the three parameters for Yeoh's model C_1, C_2 and C_3 as well as ϵ_r with a ramp input where the viscoelastic oscillation has less influence. Initial values of the parameters to be estimated are listed in Table II. The viscoelastic parameters are chosen randomly. The initial state variables are $x(0) = \begin{pmatrix} x_1(0) & x_2(0) & x_3(0) & x_4(0) \end{pmatrix}^T = \begin{pmatrix} 1 & 0 & 0 & 0 \end{pmatrix}^T$.

The identification process is carried out with the nonlinear graybox in *System Identification toolbox* of *Matlab*. The identification method is chosen to be 'lsqnonlin', and the solver is 'ode45'. We first fix the two coefficients C_2 and C_3 and only identify C_1 and ϵ_r with input signals shown in Fig. 7a. This simplification is reasonable because C_2 and C_3 has less influence for the small deformation with input voltage of 4kV. The comparison between the identified results and the experimental results of center point deformation is shown in Fig. 7b. One can notice that with the identification process, our model fits well the experimental results with an accuracy of 96.99%. The identified C_1 is therefore 333.056 kPa and ϵ_r is 2.8.

TABLE II: Initial values of the parameters to be estimated.

Names	Parameters	Values	Units
Yeoh's coefficient	C_1	195	kPa
Yeoh's coefficient	C_2	-1.5	kPa
Yeoh's coefficient	C_3	2.5	kPa
Relative dielectric permittivity	ϵ_r	$[2.8, 3.1]$	
Damping of σ_η	η_o	500	kPa · s
Stiffness of σ_{vis1}	k_1	10	MPa
Damping of σ_{vis1}	η_1	500	kPa · s
Stiffness of σ_{vis2}	k_2	10	MPa
Damping of σ_{vis2}	η_2	500	kPa · s

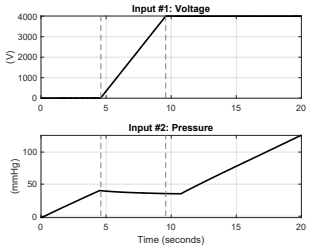

(a) Ramp inputs to the tubular DEA.

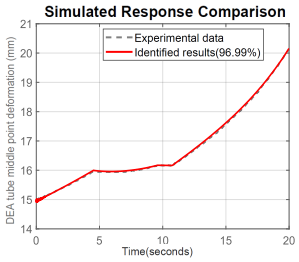

(b) Comparison of experiment with the identification.

Fig. 7: Identification with a ramp input (input voltage amplitude = 4 kV).

Next we identify C_2 and C_3 with large deformation and especially taking into account the snap-through effect. The pneumatic system follows the same dynamic as in the previous experiment. Input pressure is thus similar to Fig. 7a before the snap-through effect. The amplitude of input voltage after 9.56 s changes to 7kV. According to Fig. 8a, there is a huge discrepancy between the simulation results and the experimental one when the deformation is larger than 18.5 mm, which indicates that the identified C_1 and ϵ_r together with the initial guess of C_2 and C_3 are not precise to predict the large deformation with high applied voltage. Following the same system identification algorithm, and fixing the initial values of C_1 and ϵ_r as identified previously, the comparison between the experimental center point displacement and the simulation one is shown in Fig. 8b, with the new identified parameters C_2 being -32.5032 kPa and C_3 being 2.86041 kPa. The model now can better simulate the snap-through effect with a good fitting of 95.7%. The deformation strain along λ_2 direction is 100%. We now focus on the relation between applied pressure and the middle

point deformation of the tubular DEA after 9.56 s when the input voltage becomes constant. From the red circle of Fig. 9, when the deformation is larger than 24 mm, the tubular DEA undergoes a huge displacement with a small increase of pressure. As mentioned in the Introduction, the snap-through effect comes from the relation between the input electric field and the system output, i.e. the deformation of the DEA. According to [4], the relation has multiple equilibrium point, some of which are unstable such that the DEA can jump from one equilibrium state to another, thus leading to the snap-through phenomenon. In order to avoid this effect, it is possible to change the number of the equilibrium state and to modify the stability of unstable ones [34], which will be our next step on this tubular DEA model.

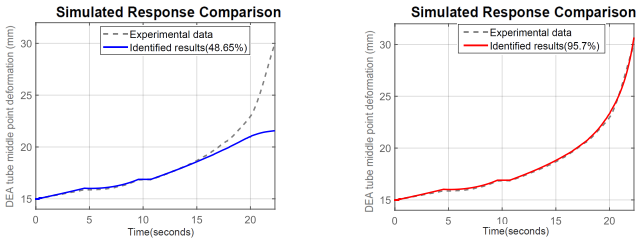

(a) Comparison before the identification of C_2 and C_3.

(b) Comparison after the identification of C_2 and C_3.

Fig. 8: Identification with a ramp input (input voltage amplitude $= 7$ kV).

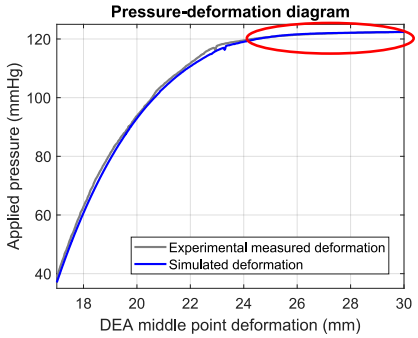

Fig. 9: Relation between the pressure and middle point deformation of the DEA after 9.56 s.

After the identification of C_1, C_2, C_3 and ϵ_r, we will investigate the visco damper and viscoelastic elements and their influence on the tubular DEA at high frequency. Therefore, the tubular DEA is firstly pre-stretched with a constant pressure of 95mmHg, and then activated with a step input voltage of 4 kV. The voltage is then removed after 10 s. Input profiles are illustrated in Fig. 10a. The identified hyperelastic parameters C_1, C_2 and C_3 as well as ϵ_r are fixed. Following the same identification procedure, we obtain the comparison between the identified center point deformation and the experimental one as depicted in Fig. 10b. With the identified parameters summarized in Table. III, the response time and the deformation at steady state of the simulation results fit well the experimental data with an accuracy of 96.31%. The oscillations around 0.7 s is zoomed in Fig. 10b. This is due to the viscoelastic properties of the elastomer. Moreover, according to this figure the tubular DEA returns to its initial position after the discharge.

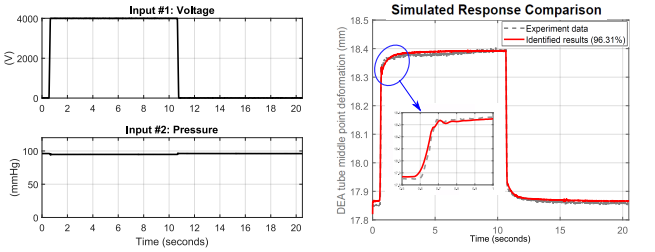

(a) Step inputs to the tubular DEA.

(b) Comparison of experiment with the identification.

Fig. 10: Identification with a step input (input voltage amplitude $= 4$ kV).

TABLE III: Identified values of the parameters.

Names	Parameters	Values	Units
Yeoh's coefficient	C_1	333.056	kPa
Yeoh's coefficient	C_2	-32.5032	kPa
Yeoh's coefficient	C_3	2.86041	kPa
Relative dielectric permittivity	ϵ_r	2.8	
Damping of σ_η	η_o	745.854	kPa $\cdot$ s
Stiffness of σ_{vis1}	k_1	19.6758	MPa
Damping of σ_{vis1}	η_1	6495.68	kPa $\cdot$ s
Stiffness of σ_{vis2}	k_2	2.414	MPa
Damping of σ_{vis2}	η_2	6508.21	kPa $\cdot$ s

To validate the identified parameters as listed in Table. III, we have also compared the simulation results of the middle point deformation of the tubular DEA with different applied voltage of amplitude of 5 kV, 5.5 kV and 6 kV, respectively. The simulation results are illustrated in Fig. 11a and Fig. 11b with voltage profile of ramp and step inputs. According to the following comparisons and the calculated goodness of fit value, the identified model has a very good agreement with the ramp input of more than 90.27%. The simulation results of step input are not as accurate as the ramp inputs, but the accuracy is still more than 82.7% as depicted in Fig. 11b. One can notice a small discrepancy of response time between the identified deformation of the tube and the experimental measurement from Fig. 11b. Another identification process of step input has been performed with three viscoelastic elements in (18). However, the goodness of fit value does not improve compared to Fig. 10b. Therefore, one possible reason for the discrepancy may be the non-linearity of viscoelastic of visco damper element that is not considered in the current model.

IV. CONCLUSIONS

In this paper we have proposed a nonlinear dynamic model for the tubular DEA. Different from the existing work, the deformation of our tubular DEA model is more complex compared to similar tubular actuators. Both the radial deformation and the circumferential force are considered in the

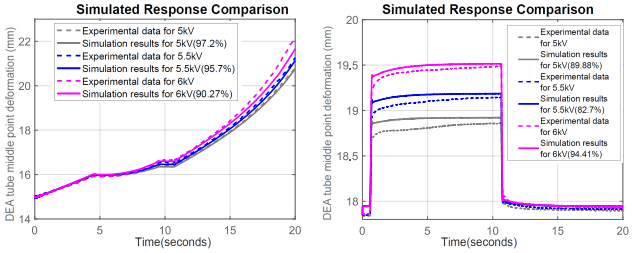

(a) Ramp inputs with voltage amplitude of 5 kV, 5.5 kV and 6 kV, respectively.

(b) Step inputs with voltage amplitude of 5 kV, 5.5 kV and 6 kV, respectively.

Fig. 11: Validations of the identified parameters.

nonlinear and multiphysical model. Moreover, our dynamic model succeeds in simulating the snap-through effect with a high voltage applied to the DEA tube as illustrated in Fig. 8b. Both the hyperelastic and viscoelastic properties of the DEA are taken into account and validated in experiment with two types of input. Apart from the application to cardiac assist device, our model of tubular DEAs can be adapted to other soft bio-medical robotics systems such as the peristaltic micro-pump to deliver medicine inside the human body. For the control design aspect, the next step will be to investigate this snap-trough effect with the established dynamic model and propose a controller in order to modify the equilibrium point of the system and to avoid this electro-mechanical instability. From the modeling point of view, we have simplified the tubular DEA with a one DOF that concentrates only on the center point deformation of the tube. This simplification helps to facilitate the stability analysis and control design. Once the controller is validated, a more precise model of multiple DOFs will be considered.

References

[1] R. E. Pelrine, R. D. Kornbluh, and J. P. Joseph, "Electrostriction of polymer dielectrics with compliant electrodes as a means of actuation," *Sensors and Actuators, A: Physical*, vol. 64, no. 1, pp. 77–85, 1998.

[2] U. Gupta, L. Qin, Y. Wang, H. Godaba, and J. Zhu, "Soft robots based on dielectric elastomer actuators: a review," *Smart Materials and Structures*, vol. 28, no. 10, p. 103002, oct 2019.

[3] M. Almanza, F. Clavica, J. Chavanne, D. Moser, D. Obrist, T. Carrel, Y. Civet, and Y. Perriard, "Feasibility of a Dielectric Elastomer Augmented Aorta," *Advanced Science*, vol. 8, no. 6, 2021.

[4] J. Zhu, S. Cai, and Z. Suo, "Nonlinear oscillation of a dielectric elastomer balloon," *Polymer International*, vol. 59, no. 3, pp. 378–383, 2010.

[5] L. Dorfmann and R. W. Ogden, "Instabilities of soft dielectrics," *Philosophical Transactions of the Royal Society A: Mathematical, Physical and Engineering Sciences*, vol. 377, no. 2144, p. 20180077, may 2019.

[6] Z. Liu, A. McBride, B. L. Sharma, P. Steinmann, and P. Saxena, "Coupled electro-elastic deformation and instabilities of a toroidal membrane," *Journal of the Mechanics and Physics of Solids*, vol. 151, p. 104221, jun 2021.

[7] R. Baumgartner, A. Kogler, J. M. Stadlbauer, C. C. Foo, R. Kaltseis, M. Baumgartner, G. Mao, C. Keplinger, S. J. A. Koh, N. Arnold, Z. Suo, M. Kaltenbrunner, and S. Bauer, "A Lesson from Plants: High-Speed Soft Robotic Actuators," *Advanced Science*, vol. 7, no. 5, p. 1903391, mar 2020.

[8] T. Martinez, J. Chavanne, A. Walter, Y. Civet, and Y. Perriard, "Design and modelling of a tubular dielectric elastomer actuator with constrained radial displacement as a cardiac assist device," *Smart Materials and Structures*, aug 2021.

[9] Z. Suo, "Theory of dielectric elastomers," *Acta Mechanica Solida Sinica*, vol. 23, no. 6, pp. 549–578, dec 2010.

[10] G. Mao, X. Huang, J. Liu, T. Li, S. Qu, and W. Yang, "Dielectric elastomer peristaltic pump module with finite deformation," *Smart Materials and Structures*, vol. 24, no. 7, 2015.

[11] T. Lu, L. An, J. Li, C. Yuan, and T. Wang, "Electro-mechanical coupling bifurcation and bulging propagation in a cylindrical dielectric elastomer tube," *Journal of the Mechanics and Physics of Solids*, vol. 85, pp. 160–175, dec 2015.

[12] A. Ghosh and S. Basu, "Soft dielectric elastomer tubes in an electric field," *Journal of the Mechanics and Physics of Solids*, vol. 150, no. January, 2021.

[13] J. Zhu, S. Cai, and Z. Suo, "Resonant behavior of a membrane of a dielectric elastomer," *International Journal of Solids and Structures*, vol. 47, no. 24, pp. 3254–3262, 2010.

[14] K. Kadooka, H. Imamura, and M. Taya, "Experimentally verified model of viscoelastic behavior of multilayer unimorph dielectric elastomer actuators," *Smart Materials and Structures*, vol. 25, no. 10, p. 105028, oct 2016.

[15] G. Rizzello, P. Loew, L. Agostini, M. Fontana, and S. Seelecke, "A lumped parameter model for strip-shaped dielectric elastomer membrane transducers with arbitrary aspect ratio," *Smart Materials and Structures*, vol. 29, no. 11, 2020.

[16] G. Rizzello, D. Naso, A. York, and S. Seelecke, "Modeling, identification, and control of a dielectric electro-Active polymer positioning system," *IEEE Transactions on Control Systems Technology*, vol. 23, no. 2, pp. 632–643, 2015.

[17] J. Zou and G. Gu, "Feedforward Control of the Rate-Dependent Viscoelastic Hysteresis Nonlinearity in Dielectric Elastomer Actuators," *IEEE Robotics and Automation Letters*, vol. 4, no. 3, pp. 2340–2347, jul 2019.

[18] J. Bernat, J. Koota, and S. Rosset, "Identification of a Nonlinear Dielectric Elastomer Actuator Based on the Harmonic Balance Method," *IEEE/ASME Transactions on Mechatronics*, vol. 14, no. 8, 2020.

[19] J. Prechtl, J. Kunze, S. Nalbach, S. Seelecke, and G. Rizzello, "Soft robotic module actuated by silicone-based rolled dielectric elastomer actuators: modeling and simulation," in *Electroactive Polymer Actuators and Devices (EAPAD) XXII*, Y. Bar-Cohen, Ed., vol. 11375, International Society for Optics and Photonics. SPIE, 2020, pp. 276 – 286.

[20] J. Prechtl, J. Kunze, D. Bruch, S. Seelecke, and G. Rizzello, "Modeling and parameter identification of rolled dielectric elastomer actuators for soft robots," in *Electroactive Polymer Actuators and Devices (EAPAD) XXIII*, I. A. Anderson, H. R. Shea, and J. D. W. Madden, Eds., vol. 11587, International Society for Optics and Photonics. SPIE, 2021, pp. 204 – 212.

[21] J. A. J.-M. Chavanne, "Cylindrical Dielectric Elastomer Actuator for Cardiac Assist Device," Ph.D. dissertation, EPFL, Lausanne, 2019.

[22] M. Wissler and E. Mazza, "Modeling of a pre-strained circular actuator made of dielectric elastomers," *Sensors and Actuators A: Physical*, vol. 120, no. 1, pp. 184–192, apr 2005.

[23] W. Hong, "Modeling viscoelastic dielectrics," *Journal of the Mechanics and Physics of Solids*, vol. 59, no. 3, pp. 637–650, mar 2011.

[24] C.-J. Cao, T. L. Hill, A. T. Conn, B. Li, and X. Gao, "Nonlinear Dynamics of a Magnetically Coupled Dielectric Elastomer Actuator," *Physical Review Applied*, vol. 12, no. 4, p. 044033, oct 2019.

[25] J. Sheng, H. Chen, L. Liu, J. Zhang, Y. Wang, and S. Jia, "Dynamic electromechanical performance of viscoelastic dielectric elastomers," *Journal of Applied Physics*, vol. 114, no. 13, 2013.

[26] M. Kollosche, G. Kofod, Z. Suo, and J. Zhu, "Temporal evolution and instability in a viscoelastic dielectric elastomer," *Journal of the Mechanics and Physics of Solids*, vol. 76, pp. 47–64, 2015.

[27] S. E. Chen, Z. C. He, and E. Li, "Comparisons between the dynamic and quasi-static performances of a dissipative dielectric elastomer under pure shear mode," *Smart Materials and Structures*, vol. 26, no. 10, 2017.

[28] Z. Wang, B. He, Y. Zhou, R. Shen, and G. Li, "Effects of pre-stretch on the oscillation and stability of dielectric elastomers," *International Journal of Mechanical Sciences*, vol. 185, no. June, 2020.

[29] M. Tewary and T. Roy, "Nonlinear actuation of non-prismatic dielectric elastomeric membrane," *Soft Materials*, vol. 19, no. 1, pp. 1–23, 2021.

[30] G. Rizzello, D. Naso, and S. Seelecke, "A Thermodynamically Consistent Port-Hamiltonian Model for Dielectric Elastomer Membrane

Actuators and Generators," *IFAC-PapersOnLine*, vol. 50, no. 1, pp. 4855–4862, jul 2017.

[31] C. R. Kelley and J. L. Kauffman, "Tremor-Active Controller for Dielectric Elastomer-Based Pathological Tremor Suppression," *IEEE/ASME Transactions on Mechatronics*, vol. 25, no. 2, pp. 1143–1148, 2020.

[32] T. Nguyen, J. Li, L. Sun, D. Tran, and F. Xuan, "Viscoelasticity modeling of dielectric elastomers by kelvin voigt-generalized maxwell model," *Polymers*, vol. 13, no. 13, 2021.

[33] O. H. Yeoh, "Some Forms of the Strain Energy Function for Rubber," *Rubber Chemistry and Technology*, vol. 66, no. 5, pp. 754–771, nov 1993.

[34] L. Hines, K. Petersen, and M. Sitti, "Asymmetric stable deformations in inflated dielectric elastomer actuators," in *2017 IEEE International Conference on Robotics and Automation (ICRA)*, 2017, pp. 4326–4331.